



Numerical Analysis of CHS Unstiffened Bolted Circular Flange Connection

Moamen Emara¹, Ezzeldin Sayed-Ahmed², and Emam Soliman³

¹Structural Engineering department, Ain Shams University, Cairo, Egypt

²Department of Construction Engineering, The American University in Cairo, Cairo, Egypt

³Structural Engineering department, Ain Shams University, Cairo, Egypt

ملخص البحث

تتواجد القطاعات الدائرية المفرغة بشكل ملحوظ في الطبيعة، وذلك لكفاءتها العالية حيث تجمع بين صفات إنشائية مميزة وفي نفس الوقت تستخدم مساحة سطحية أقل مقارنة بأنواع أخرى من القطاعات. وكنتيجة لهذه المميزات وبالإضافة إلى مظهرها اللائق معماريا تستخدم القطاعات الدائرية المفرغة في العديد من التطبيقات الإنشائية، ولكن بالرغم من خصائصها المميزة فإن التعامل مع وصلاتها يعد أكثر تعقيدا ويتطلب إجراء العديد من التحليلات العددية أو العملية في بعض الأحوال للتنبؤ بسلوكها. وقد أصبحت وصلات المسامير أحد أهم الحلول لوصل هذه الأعضاء الإنشائية حيث توفر هذه الوصلات سرعة وسهولة في التركيب دون الحاجة إلى إجراء أي لحامات حقلية. وعادة ما تتعرض الأعضاء الإنشائية ذات القطاعات المفرغة إلى تحميل محوري بالإضافة إلى عزوم الانحناء ولقد درس العديد من الباحثين مقاومة هذه الوصلات القصوى للأحمال المحورية حيث تعطي المراجع معادلات التصميم والحسابات للوصلات المعرضة لتحميل محوري بصوره تفصيلية. أما عند تعرضها لعزوم انحناء فيعتمد التصميم على افتراض حمل محوري مكافئ لقوى الشد الناتجة عن عزوم الانحناء، وقد اعتمده بعض الاكواد للتصميم وهو ما يعتبر تصميمًا متحفظًا لهذه الوصلات. وتهدف هذه الورقة البحثية الى دراسة سلوك هذه الوصلات المفرغة باستخدام الألواح الدائرية المعرضة لعزوم انحناء عن طريق التمثيل السليم للوصلة تحت الدراسة باستخدام التحليل العددي تمهيدا لاستخدامه في إيجاد معادلات تصميمية لهذا النوع من الوصلات.

الكلمات الدلالية: قطاعات دائرية مفرغة، وصلات المسامير، وصلات مقاومة للعزوم، التحليل العددي.

ABSTRACT

Circular hollow section is very efficient, as it combines interesting structural features and using less material than other sections. Combined with an architecturally appealing shape, circular hollow sections are commonly used in structures. However, treatment of their connections is complex and requires empirical and numerical tests to predict their behaviour. Unlike the behaviour of this joint when subjected to axial force, which is extensively studied before, very few researches have been performed on its behaviour under the effect of bending moment, leading to an approximate design approach adopted by current codes of practice. Thus, this research aims to scrutinize the behaviour of the bolted circular CHS joints subjected to pure bending moment. A non-linear numerical model is developed using a general-purpose finite element analysis (FEA) package, known as Abaqus. The model is verified against an experimental program found in literature and good correlation between results is found. After the verification, the model will be prepared to be used with confidence in a parametric study to determine the capacity and behaviour of different configurations of the joint.

Keywords: circular hollow sections, CHS, bolted connections, moment connections, CHS splice, numerical modelling, Abaqus, FEA.

INTRODUCTION

Bolted flange-plate connections, shown in Figure 1, is becoming increasingly popular as an efficient solution for splicing steel tubular structures. These connections provide easy and fast installation, appealing shape, and simple composition without the need for field welding. Axial loading is usually developed in steel tubular trusses, while bending moment often appears when structures sustain lateral loads such as those resulting from wind or seismic. Current researches only investigated axial load design calculation. For

tensile-flexure case, design is based on superposition where an effective axial load can be computed which is, at most, a conservative approximation. This situation restricts the generalization of these connections. Consequently, it is important to do further study on the behaviour of head plate connections under bending moment.

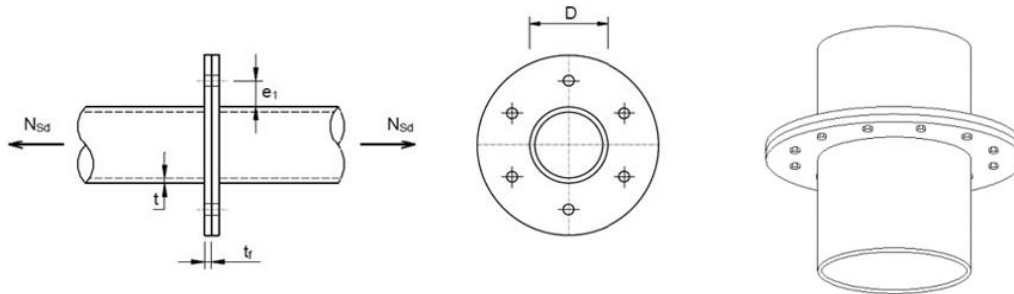


Figure 1 Bolted flange-plate connection under axial load

Couchaux et al. (2011) proposed an analytical model to determine the static resistance of bolted circular flange joint under a combination of bending moment and axial load, whether tension or compression. Both ductile and non-ductile failure modes were considered, based on the ductility of compressive and tensile parts of the joint. All the components reach their plastic resistance when the ductile failure mode was considered, while only the highest stressed component locally reached its resistance when considering non-ductile failure. The finite element model used considered an elastic-plastic behaviour and non-linear contact elements to perform a parametric study, which was used to verify the derived analytical model.

Couchaux et al. (2012) proposed a model to determine the global behaviour, elastic and elastic-plastic, of a circular flanged joint subjected to a combination of bending moment and axial force, tension or compression. The authors were concerned with the joint rotational stiffness and its moment-rotation curve to fully estimate the behaviour of this type. The proposed analytical model, based on component method, predicting the behaviour was then compared to the finite element analysis model (Couchaux et al. 2011) and experimental results and a good correlation was found.

Wang et al. (2013) study was focused on behaviour of flanged joints of hollow sections subjected to pure bending. The authors were concerned with four basic types of connections namely; unstiffened circular flanged joints, stiffened circular flanged joints, unstiffened rectangular flanged joints, and stiffened rectangular flanged joints, as shown in Figure 2. The authors performed finite element analysis to analyse the connection and revealed the strains and contact pressures at flanges. Experimental tests were performed to verify the numerical models. The result of the numerical model was used to predict the yield line mechanisms and pressure centre in the theoretical model. The virtual work method was then used to determine the flanges bending capacity. T-stub analogy was also used to determine the bolts capacity. Practical design procedures were concluded combining both T-stub analogy and yield line analysis design approach. The new procedures were limited to bolted flanged joints with eight bolts.

CURRENT DESIGN APPROACH

Most Design standards does not address the design of this type of connection, including, but not limited to, Egyptian Code of Practice. Few design guides address the design of these joints, and mostly against tensile loads only, and computing a hypothetical

“effective” axial load in case of bending moment (Kurobane et al. 2004), which is, at most, a conservative approximation.

$$Effective\ axial = \left(\frac{N_i}{A_i} + \frac{M_i}{W_i} \right) A_i$$

Where,

N_i = Axial force acting on member

M_i = Bending moment acting on member

A_i = cross sectional area of the CHS

W_i = elastic (or plastic) section modulus of the CHS

CIDECT

Wardenier et al. (2008) proposed a design method in CIDECT Design Guide 1 based on Igarashi et al. (1985), where the flange plate thickness, shown in Figure 4, can be calculated from:

$$t_f = \sqrt{\frac{2 N_i \gamma_M}{f_{yp} \pi f_3}}$$

And number of bolts (n) can be determined from:

$$n \geq \frac{N_i \left[1 - \frac{1}{f_3} + \frac{1}{f_3 \ln(r_1/r_2)} \right]}{0.67 T_u} \gamma_M$$

Where,

N_i = tensile member force

f_{yp} = yield strength of plate

$\gamma_M = 1.1$ (partial safety factor)

f_3 = dimensionless factor to be obtained from Figure 3

t_f = thickness of flange plate

T_u = ultimate tensile resistance of a bolt

$r_1 = 0.5d_i + 2e_1$

$r_2 = 0.5d_i + e_1$

The dimension e_1 is recommended to be kept minimum, around $1.5 d_i$ to $2 d_i$, to minimize prying force, while taking into account a weld-nut clearance of at least 5 mm.

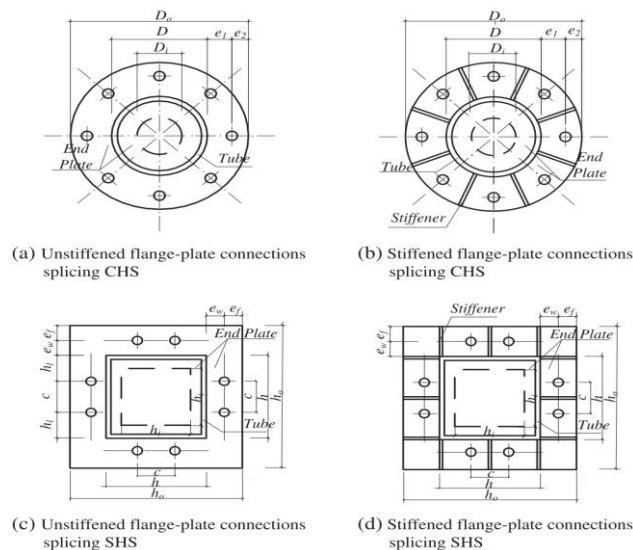


Figure 2 Four basic types of flange-plate connections with 8 bolt

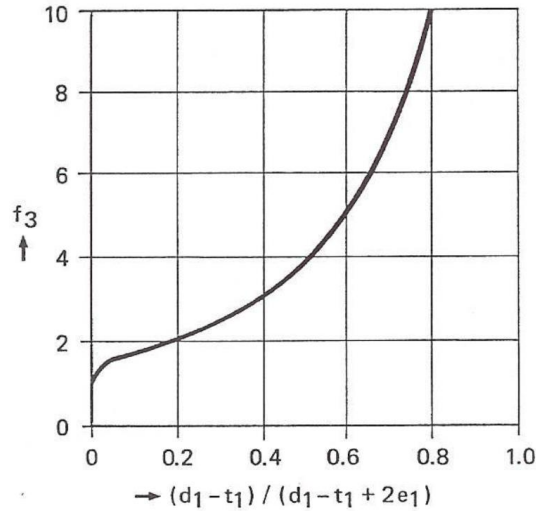


Figure 3 Parameter f3 for use in the design of CHS flange plate joints in CIDECT

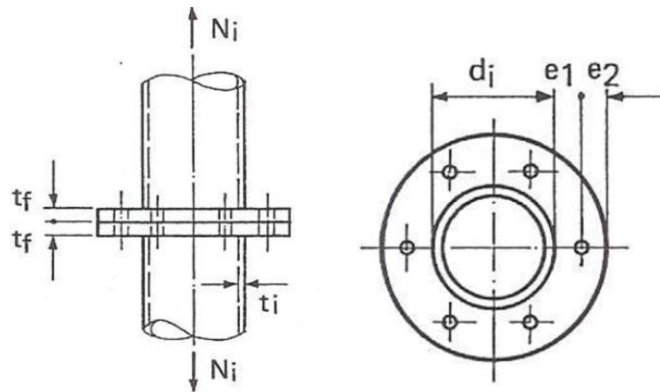


Figure 4 Circular Flange Joint subjected to tensile stresses in CIDECT

AISC

Packer et al. (2010) followed a similar approach to CIDECT design guide in AISC Design Guide 24, where the authors considered the following limit states:

- End-plate yielding

- Tensile strength of the bolts, considering prying action

- Strength of the weld connecting the end-plate to the CHS

Due to the complexity inherited in the behaviour of the connection resulting from prying action, using AISC specification provisions to directly determine nominal resistance is difficult. Hence, the design follows equations presented by Packer and Henderson (1997) to determine the flange plate thickness, number of bolts, and size of weld:

$$t_p \geq \sqrt{\frac{2P_r}{c F_{yp} \pi f_3}}$$

$$n \geq \frac{P_r}{R_c} \left[1 - \frac{1}{f_3} + \frac{1}{f_3 \ln(r_1/r_2)} \right]$$

$$w \geq \frac{P_r \sqrt{2}}{F_{wc} \pi D}$$

Where,

D = CHS outside diameter, in.

F_{yp} = specified minimum yield stress of the plate, ksi

P_r = required strength using LRFD or ASD load combinations, as applicable, kips; for LRFD, $P_r = P_u$; for ASD, $P_r = P_a$

R_c = available tensile strength of a bolt using LRFD or ASD load combinations, as applicable, kips; for LRFD, $R_c = \phi r_n$; for ASD, $R_c = r_n / \Omega$

F_{wc} = available weld strength using LRFD or ASD load combinations, as applicable, kips; for LRFD, $F_{wc} = \phi F_w$; for ASD, $F_{wc} = F_w / \Omega_w$

$c = \phi$ for LRFD; $1 / \Omega$ for ASD

$f_3 = \frac{1}{2k_1} \left(k_3 + \sqrt{k_3^2 - 4k_1} \right)$, or can be determined using a chart similar to Figure 3.

$$k_1 = \ln(r_2/r_3)$$

$$k_3 = k_1 + 2$$

$$r_1 = \frac{D}{2} + 2b$$

$$r_2 = \frac{D}{2} + b$$

$$r_3 = \frac{D - t}{2}$$

a, b, D, and t are shown in Figure 5

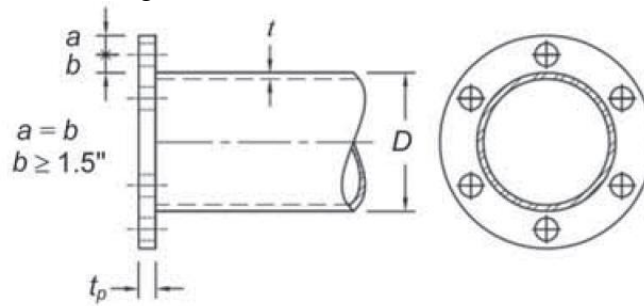


Figure 5 Circular Flange Joint subjected to tensile stresses in AISC

NUMERICAL MODELING

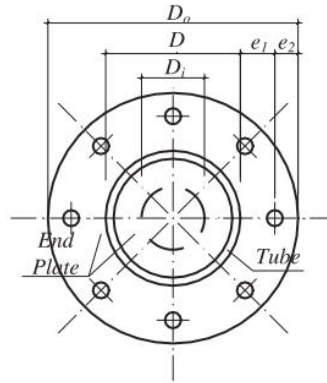
To simulate the behavior and failure moment of the connection, a non-linear finite element model is developed using a general FEA software package, known as ABAQUS/CAE and later verified against experimental data.

MODEL ASSEMBLY

The finite model follows closely the configuration and parameters of the experimental program by Wang et al. (2013). The program included four types of joints. The one of interest is the unstiffened flange-plate joint splicing CHS, shown in Figure 6, where it is used for the verification of this Finite element model.

The size of CHS pipe used in the study is $\phi 168 \times 10$ mm of a Chinese steel grade Q345B, equivalent to Eurocode grade S355. The end-plate used is a ring plate with inner diameter of $\phi 118$ mm and outer diameter of $\phi 312$ mm. $8 \times M24$ bolts are used for each joint. Bolts are of grade 8.8S with an engineering yield stress of 660 MPa and an ultimate stress of 800 MPa. The bolt internal and external edge distances are kept fixed at the recommended $1.5 \times$ bolt diameter; 36 mm. The end-plate is 16 mm thick with a steel grade Q345B. The beam length is 2 m, simply supported on both ends, spliced by bolted flanged joints at midspan. The load is applied at the quarters of the beam, resulting in pure bending load on the beam. Circular internal stiffeners are added

at both end of the pipe to prevent local buckling at support locations. Also, to simulate the load application points, two internal stiffeners at the quarters of beam, as shown in Figure 7.



(a) Unstiffened flange-plate connections splicing CHS

Figure 6 Unstiffened CHS joint configuration used in experimental program



Figure 7 Finite element model of unstiffened joint

ELEMENTS USED

CHS pipe and end-plates are all modelled using shell elements with six degrees of freedom at each node; three translational and three rotational degrees. Element type S4 is used, which is 4-node doubly curved general-purpose shell element with finite member strains. This element has four integration points, as shown in Figure 8. Since this element does not exhibit hourglass modes, no need for hourglass control. As this element account for finite membrane strains and arbitrarily large rotations, they are recommended by ABAQUS/CAE for large-strain analysis as the change in thickness with deformation results from the Poisson's effect. Being a general-purpose shell element, it is suited for both thick and thin shell, as it allows transverse shear deformation; it uses thick shell theory as the shell thickness increases and become discrete Kirchhoff thin shell elements as the thickness decreases; the transverse shear deformation becomes very small as the shell thickness decreases. Gauss quadrature with 3 points is used for shell section thickness integration, as it is less computationally expensive than Simpson's rule given the same level of accuracy. Mesh sizes range from 20 mm in CHS pipe to 3 mm in end-plate to capture any stress concentration and give accurate and reliable results.

Bolts are simulated using beam elements. Beam length is taken as double the end-plate thickness to simulate the axial stiffness and strain of bolts correctly. Beam cross-section is taken as circular profile with a diameter equals to the diameter of the bolt shank. A 2-node linear beam in 3D, shown in Figure 9, is used allowing six degrees of freedom at beam end nodes; three translational and three rotational degrees. To capture the behaviour of bolts accurately, the beam elements are meshed to a size of 2 mm.

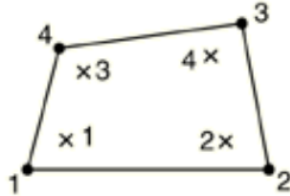


Figure 8 four-node full integration element (S4)



Figure 9 Two node linear element integration point

MATERIAL MODEL

Wang et al. (2013) proposed the use of multilinear material model with yield plateau for the end-plate and tube, shown in Figure 10a, while the use of bi-linear material model for high strength bolts, shown in Figure 10b.

The “engineering” material data found in the experimental study is used in the FEM after converting the data into true stresses and true plastic strains to suit ABAQUS input, through the following equations:

$$\begin{aligned}\sigma_t &= \sigma_e (1 + \varepsilon_e) \\ \varepsilon_t &= \ln(1 + \varepsilon_e) \\ \varepsilon_t^p &= \varepsilon_t - \frac{\sigma_t}{E}\end{aligned}$$

Von Mises yield criterion is used as it is considered suitable for the analysis of steel material (DNV 2013). It computes a single equivalent stress for steel specimen “isotropic” under the three principal stresses combined. A graphical representation of Von Mises yield criterion in case of planer loading is shown in Figure 11.

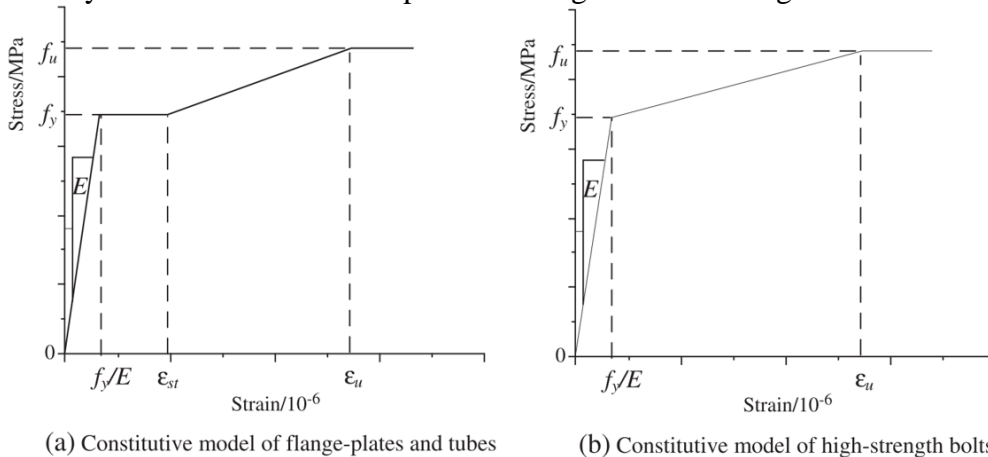


Figure 10 material model: (a) plates and CHS pipe; (b) high strength bolts.

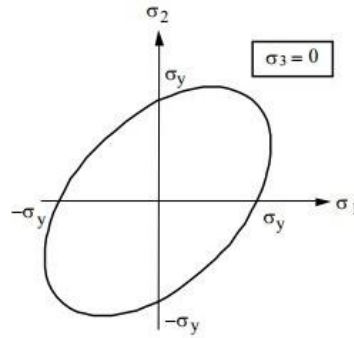


Figure 11 Von Mises yield criterion in case of 2D (planar) loading

BOUNDARY CONDITIONS

Both ends of the beam are stiffened by a cap plate, shown in Figure 14a, and only the centre point is supported. To prevent local buckling and stress concentration, the centre node is constrained to all the perimeter nodes using MPC type beam. End-supports are modelled to closely simulate the actual boundary conditions of the experimental test setup. The centre node is constrained in vertical translation (in Y-axis direction) and constrained horizontally in X-axis translation direction. No constraint is simulated in Z-axis translation direction, but torsion is restrained by constraining the rotational degree of freedom around Z-axis.

To stabilize the joint in Z-axis translation direction and enforce symmetry, a plane of symmetry is created exactly in the middle span, shown in Figure 14b. The bolt midpoint is used for the symmetry boundary conditions. For XY plane of symmetry, translation in Z-axis direction is prevented, in addition to rotation about X-axis and rotation about Y-axis. Other DOFs are not restrained in any way.

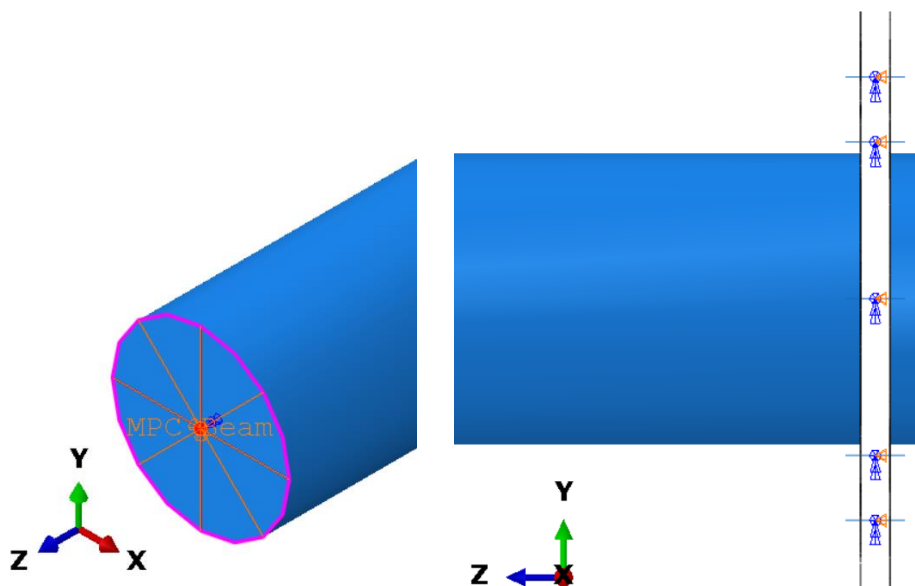


Figure 12 Boundary Conditions: (a) at beam support (left); (b) at the plane of symmetry (right)

LOAD ASSIGNMENT

The load is applied on the centre of the internal stiffener plate at quarters of the beam, coincident with CHS pipe longitudinal axis, shown in **Figure 13**, to result in pure

bending load on the beam without shear. The stiffener plate centre (load application point) is constrained to its edge by multi-point constraint type beam, shown in Figure 14, which provides a rigid beam between the central node and all edge nodes to constrain the displacement and rotation of the edge nodes to the load application point at centre to distribute the load on the CHS pipe perimeter nodes and prevent stress concentration, local buckling, and any premature failure of the internal stiffener.

CONTACT

Interaction between the two end-plates surface is simulated using surface-to-surface contact. Small-sliding formulation is used, assuming relatively small surface sliding, but can allow rotation and separation (Jayachandran et al. 2009). Normal behaviour is defined as hard contact, shown in Figure 15a, with linear penalty method, which is a stiff approximation of the hard contact, but computationally less expensive than direct method, as it approximates hard pressure-overclosure behaviour, shown in **Figure 15b**. Tangential behaviour is defined with penalty friction formulation with a friction coefficient of 0.3 (Jayachandran et al. 2009; Mashaly et al. 2011; Vegte and Makino 2004).

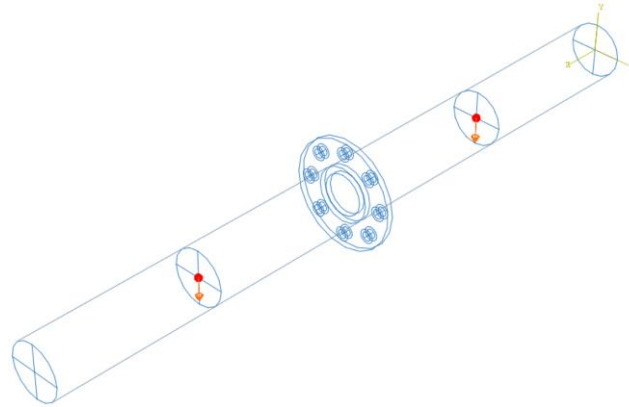


Figure 13 Load application in FEM

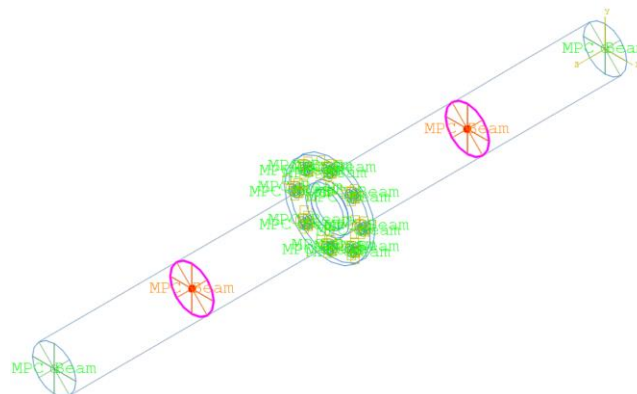


Figure 14 MPC: beam constraint at internal stiffener at load application point

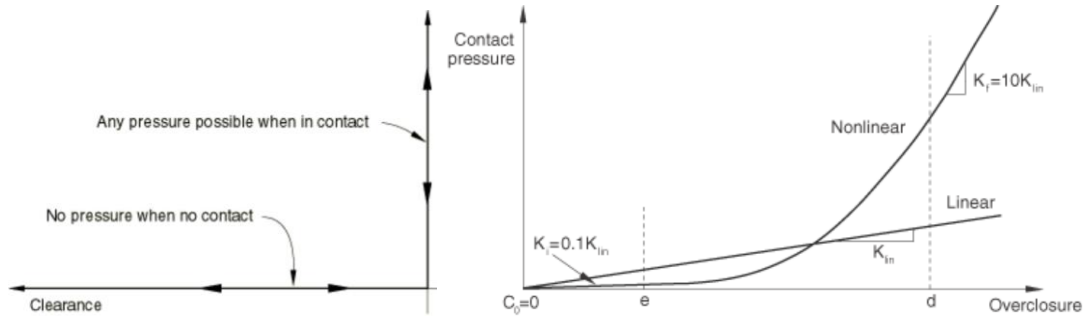


Figure 15 Contact simulation: (a) Hard Contact (left); (b) Linear and non-linear penalty method (right)

MODEL VERIFICATION

The results obtained from FEA is compared to the experimental results of Wang et al. (2013) and is used to validate and verify the FE model developed. The failure mode of this test specimen is the fracture of full penetration weld between tube and end-plate. This limits the experimental results for the loading till the weld fracture. Fortunately, the failure in weld occurs after the joint reached yield stress and demonstrated plastic deformation in the plate. The deformed shape obtained in FEM, shown in Figure 16, is realistic and reflects the true behaviour of the joint.

Figure 18 shows the load-displacement curve of the developed FEM plotted against the experimental results. It shows that there is a good agreement between the behaviour of the joint observed in tests and obtained using FEM.

As observed, the initial stiffness of FEM correlates very well with the experimental stiffness, and the first part of the curves, before yielding, is very near and difficult to distinguish.

As the weld is not modelled in the developed FEM, the ultimate moment acting on the joint cannot be compared. However, considering the weld fails at the same value of midspan deflection, we can conclude that the FEM is slightly more conservative than the experimental results, where the ultimate moment calculated using FEM is 90 kN·m while the obtained in experiment is 96 kN·m, yielding an accuracy of 94% on the conservative side, with only a 6% difference which can be attributed to fabrication error, neglect of welds, or the material model, which is not perfectly known.

It is also worth mentioning that the finite element developed by Wang et al. (2013) in parallel with the experimental program, shown in Figure 17, is modelled using computationally more expensive solid elements and its related contact yields results in a good agreement with the developed FEM, where the load-displacement curves are difficult to distinguish from each other, as shown in Figure 18. This further increases the trust in the results of the computationally less expensive model adopted for this study.

No symmetry is used in the analysis model to reduce its size to capture the true behaviour of all bolts, even bolts at the possible symmetry plane. However, Riks analysis is replaced by general static analysis, as unstable post-buckling response is not required nor expected. The adopted general static analysis yields the same behaviour and results up till ultimate load but is computationally less expensive.

CONCLUSION

A numerical model is developed to simulate the behaviour of CHS Unstiffened Bolted Circular Flange Connection. The model results correlate well with the experimental investigation results in simulating the actual joint behaviour of these connections with a good level of accuracy. The proposed model can predict the maximum capacity of the joint using less numerically demanding analysis, resulting in easier and faster simulation. Hence, this model can be used as a base for a parametric study serving toward a greater understanding of the behaviour of this type of joints and providing design recommendations for them.

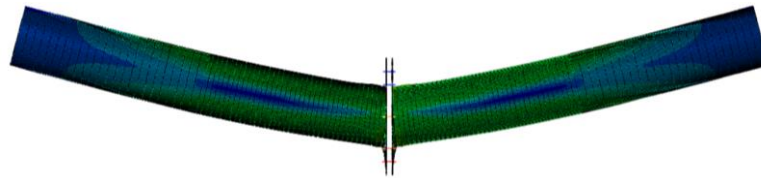


Figure 16 Deformed shape of J1 joint FEM

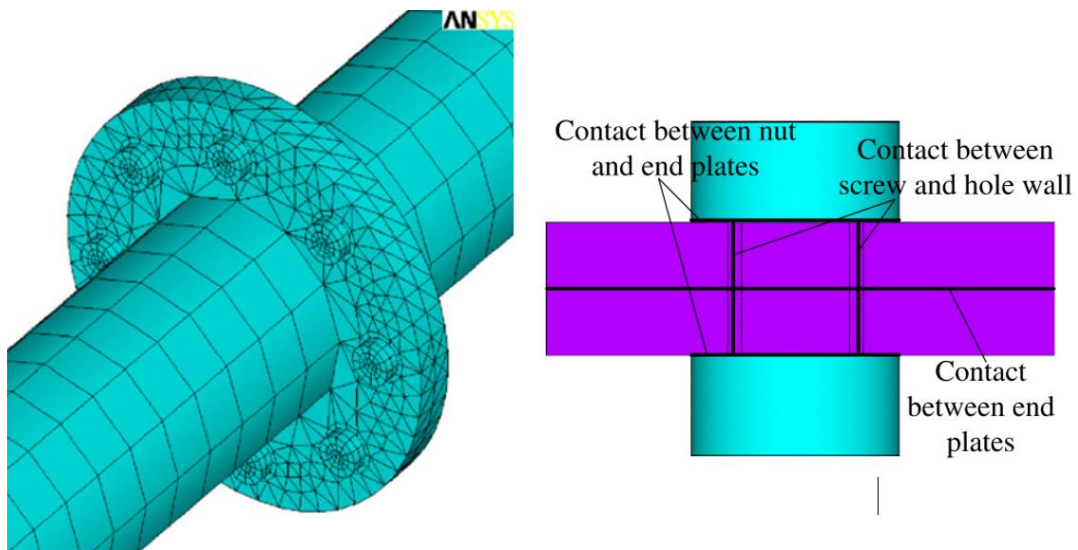


Figure 17 Reference FEM developed by Wang et al. (2013)

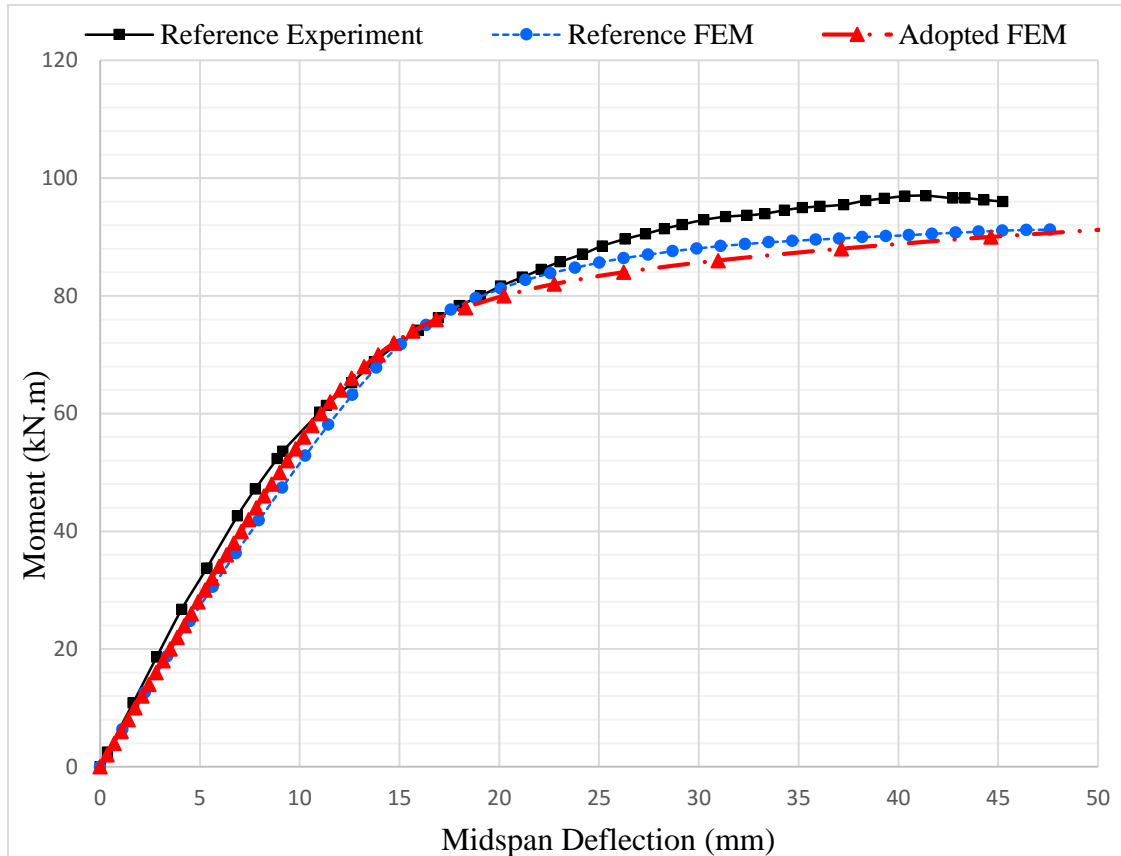


Figure 18 Load-Displacement Curve

REFERENCES

1. Emara, Moamen et al., Behaviour and design of bolted circular hollow section (CHS) moment connection, MSc thesis, Ain Shams University, 2018.
2. ABAQUS/CAE 6.14. Dassault Systèmes Simulia Corp., Providence, RI, USA.
3. Couchaux M, Hjjaj M, Ryan I. Behaviour of Bolted Circular Flange Joints Subjected to a Bending Moment and an Axial Force. 7th International Workshop on Connections in Steel Structures, 2012.
4. Couchaux M, Hjjaj M, Ryan I, Bureau A. Bolted Circular Flange Connections - Bending and Axial Static Resistance, EUROSTEEL 2011; 2011.
5. DNV. Determination of Structural Capacity by Non-linear FE analysis Methods. Dnv-Rp-C208 2013; DNV-RP-C20.
6. Igarashi S, Wakiyama K, Inoue K, Matsumoto T, Murase Y. LIMIT DESIGN OF HIGH STRENGTH BOLTED TUBE FLANGE JOINTS: Part 1. Joint without rib-plates and ring-stiffeners. Journal of Structural and Construction Engineering 1985:52–66.
7. Jayachandran SA, Marimuthu V, Prabha P, Seetharaman S, Pandian N. Investigations on the behaviour of semi-rigid endplate connections. Advanced Steel Construction 2009;5:432–51.

8. Kurobane Y, Packer JA, Wardenier J, Yeomans N. Design Guide for Structural Hollow Section Column Connections. 2004.
9. Mashaly E, El-Heweity M, Abou-Elfath H, Osman M. Finite element analysis of beam-to-column joints in steel frames under cyclic loading. Alexandria Engineering Journal 2011;50:91–104.
10. Packer JA, Henderson JE. Hollow structural section connections and trusses: A design guide. Willowdale, Ont.: Canadian Institute of Steel Construction; 1997.
11. Packer JA, Sherman DR, Lecce M. Steel Design Guide 24: Hollow Structural Section Connections. Steel Design Guide Series 2010:153.
12. Vegte G Van Der, Makino Y. Numerical simulations of bolted connections: the implicit versus the explicit approach. Connections in Steel Structures V 2004:89–98.
13. Wang YQ, Zong L, Shi YJ. Bending behavior and design model of bolted flange-plate connection. Journal of Constructional Steel Research 2013;84:1–16.
14. Wardenier J, Kurobane Y, Packer JA, Vegte GJ van der, Zhao X-L. Design guide for circular hollow section (CHS) joints under predominantly static loading. vol. 54. CIDECT; 2008. doi:10.1016/S0034-3617(10)70040-0.